Model of Stress-Induced Defect Formation in Drying Polymer Films

K. N. Christodoulou
DuPont CR&D, Wilmington, DE 19880

E. J. Lightfoot
DuPont Fluoroproducts, Buffalo, NY 14207

R. W. Powell
Dept. of Chemical Engineering, Princeton University, Princeton, NJ 08544

Photographic films are multilayer polymer structures coated from solution onto a relatively rigid substrate, chilled into a solid gel, and then dried into a permanent coating. This model predicts stress growth and defect formation during drying of such films that remain above their glass transition temperature, so that Fickian diffusion persists. The stress in the drying gel is taken from mixture theory; the polymer network is a nonlinear elastic or hypoelastic solid, whereas the solvent is an ideal fluid. Conservation laws and constitutive equations are formulated in terms of the polymer network velocity and discretized by the mixed method of Guenette and Fortin on an elliptically generated, independently evolving finite-element mesh. Results include evolution of polymer velocity, free surfaces, solvent concentration, and residual stress. Various model problems are solved for drying of uniformly coated films, suspended films (as in tenter-frame ovens) and around rigid particle inclusions in suspended films and in multilayer photographic coatings causing particle migration and drying defects.

Introduction

Thin coatings of polymer solutions are used in a variety of industrial applications, including photographic film manufacture and processing and microelectronics fabrication and packaging (Cohen, 1990). Typical coatings are applied on a substrate as liquids and are then solidified by chilling, drying, curing, or a combination thereof before attaining useful form. Volume changes that occur during the solidification process in combination with the area constraint, due to adhesion to the substrate or to other layers in the same composite, cause residual stresses in the coating. In the final coated composites, residual stresses are among the principal causes of defects such as curl, reticulation, delamination, and cracking (Cohen et al., 1990; Sato, 1980; Perera, 1984; Bierwagon, 1979). The economic impact of stress-induced defects—manifested through loss of product, productivity constraints, and impaired product performance—is on the order of billions of U.S. dollars per annum (Cohen, 1990).

The mechanisms of formation of these defects are not well understood. The best known cause of residual stress is the thermoelastic stress that arises in cooling composites with different thermal conductivities in the various layers (Nowacki, 1986). The generalization of linear thermoelasticity to include concentration effects is straightforward (Sih et al., 1986). The qualitative mechanism of residual stress arising due to solvent loss in drying has been confirmed by Croll (1979) using measurements on glassy, and thus effectively elastic, coatings. Major difficulties are encountered, however, in predicting residual stress development in drying of polymer films that have been coated and gelled from dilute solutions such as in the manufacture of photographic films. In these systems, the volume and geometry of localized defects can change drastically and the resulting deformation is too large to justify use of linear elasticity. The rheological behavior of the coatings is typically complicated by phase transitions (sol-to-gel or gel-to-glass) and, even in the absence of phase transitions, rheological and transport properties vary by orders of magnitude over the course of drying.

Correspondence concerning this article should be addressed to K. N. Christodoulou at his current address: Avery Research Center, 2900 Bradley St., Pasadena, CA 91107.

This work is the first step toward a predictive theory of stress growth and defect formation in drying of thin polymer coatings. This undertaking requires elements from disparate fields of research: rheology of mixtures of elastic solids and fluids, mass transport within the coating and in the gas phase external to it, solution thermodynamics of polymer-fluid mixtures, and large deformation analysis with associated numerical methods. While it is not practical to provide comprehensive overviews of any one of these fields here, the most pertinent results from the literature will be briefly reviewed as needed.

Many materials, particularly materials that gel into hard hydrophobic networks, develop microscopic gaseous inclusions, that is, become porous during drying. In such materials, large residual stresses arise from interfacial tension as the liquid-vapor interface retreats within the coating (Brinker and Scherer, 1990, p. 459). Mass transfer in these systems is mainly by capillarity rather than molecular diffusion (Ceaglske and Hougen, 1937). By contrast, the materials of interest in this work, such as gelatin gels, are so deformable and hydrophilic as not to support any capillary pressure. In addition, the temperature and final solvent concentration are such that mass transport during drying is usually not accompanied by the mixture's rubber-to-glass transition. Therefore, the materials dry as a single phase and non-Fickian effects such as anomalous and Case-II kinetics (Lustig, 1989) do not occur. Moreover, under certain conditions (Durning and Morman, 1993) stress-related contributions to diffusion flux can be ignored, which is then given by Fick's law.

The model developed here is based on the conservation laws of the total and the solvent mass and the total momentum together with constitutive equations (CEs) for the mixture stress and diffusive flux. The gels of interest are nearly incompressible and exhibit little or no volume change on mixing, that is, the partial specific volumes of polymer and solvent are independent of pressure and composition. However, the theory can be extended to handle compressibility effects. The stress in the drying gel is taken from Kenyon's (1976b) mixture theory to consist of an isotropic pressure and a "contact stress" due to the deformation of the polymer network. The contact stress is derived from a nonlinear elastic or more general differential hypoelastic law (Eringen, 1962).

The conservation laws CE and equations of state are conveniently expressed in terms of the velocity of the solid component and then reformulated on an elliptically generated, boundary-conforming but independently evolving finite-element mesh. The equations are discretized in space by various Galerkin and upwinded finite-element methods, and the resulting large system is integrated in time by means of a differential-algebraic system solver. The hypoelastic CE used endows the governing system with all the difficulties encountered in solving viscoelastic flow problems at a high Deborah number (Keunings, 1989) and was handled efficiently with the mixed method of Guenette and Fortin (1995).

Three sample drying problems are solved. The first and simplest, drying of a uniformly coated film, has an analytical solution that is used for model validation and for comparing residual stresses computed with various CEs. The second problem is stress development around a rigid cylindrical inclusion in a suspended film being dried from both sides as in certain stretching and drying operations in tenter-frame ovens. The third problem is prediction of stress development around a rigid spherical inclusion in a two-layer photographic coating causing particle migration and the so-called "starry night" defect, a common plaque in the photographic industry.

Governing Equations

The evolution of deformation and stress in a drying gel (polymer-solvent mixture), here assumed to be isothermal, is governed by a set of conservation laws and CEs. The overall continuity, the continuity of one component (polymer), and the overall momentum equation with negligible inertia and body forces are

$$\frac{\partial \rho}{\partial t} + \nabla\cdot(\rho \boldsymbol{v}) = 0 \tag{1}$$

$$\frac{\partial \rho_p}{\partial t} + \nabla\cdot(\rho_p \boldsymbol{v}_p) = 0 \tag{2}$$

$$\nabla\cdot\boldsymbol{T} = \boldsymbol{0} \tag{3}$$

Here, $\boldsymbol{T}$ is the Cauchy stress tensor of the mixture, $\boldsymbol{v}$ the mass-average velocity, w the solvent mass fraction, and ρ the total mixture density given by an equation of state of the form, respectively.

$$\rho = \rho(p_f, w) = \frac{1}{w/d_w + (1-w)/d_p}. \tag{4}$$

Here d_w and d_p are the inverse partial specific volumes of solvent and polymer and may depend on $\boldsymbol{T}$ and on w; $\rho_p = \rho(1-w)$ is the polymer density and $\boldsymbol{v}_p$ the polymer velocity. The set (Eqs. 1–4) is closed by constitutive equations for $\boldsymbol{T}$, and for the diffusive flux $\boldsymbol{j} \equiv \rho_p(\boldsymbol{v} - \boldsymbol{v}_p)$, both of which will be specified in detail below.

Common boundary conditions for the system (Eqs. 1–3) are: on all rigid boundaries, specification of polymer velocity (no slip); at free surfaces, vanishing air friction, capillarity, and polymer flux, along with solvent flux (or evaporation rate) characterized by a mass-transfer coefficient k_m. The free surface stress condition, equations for the polymer flux (kinematic condition) and for the total flux at a free surface are

$$\boldsymbol{n}\cdot\boldsymbol{T} = \boldsymbol{0} \tag{5}$$

$$\boldsymbol{n}\cdot(\boldsymbol{v}_p - \dot{\boldsymbol{x}}_{FS}) = 0 \tag{6}$$

$$\boldsymbol{n}\cdot(\boldsymbol{v} - \dot{\boldsymbol{x}}_{FS}) = k_m(y_s - y_\infty) = k_m H(w_s - w_\infty) \tag{7}$$

where $\dot{\boldsymbol{x}}_{FS}$ is the velocity of the free surface; $\boldsymbol{n}$ is the local unit normal to the free surface; y_s and y_∞ are the water mole fractions in the air just above the gel surface and far away from the surface; and H is a Henry's law coefficient, which relates water mass fractions in the gel w with water mole fractions in the air y at equilibrium.

Diffusive flux

Solvent transport in polymers causes rearrangement of the macromolecular chains to conformations consistent with the new penetrant concentration. If this chain rearrangement occurs on a time scale comparable to that of diffusion, such as

when accompanied by the mixture's glass transition, significant changes in its mechanical and transport properties occur and non-Fickian diffusion kinetics result (Vrentas et al., 1975; Lustig, 1989). In photographic film coating, however, the temperature and solvent concentration during drying are usually such that the mixture remains above its glass transition. Therefore, a single (rubbery) phase persists and non-Fickian effects do not occur. Such Fickian diffusion regimes in polymers have been classified by Vrentas et al. (1986) as "elastic," "viscous," or "rubbery elastic" after the corresponding regions in the linear complex modulus vs. frequency plot. Photographic coatings are gelled before and during drying, so the diffusion mechanism is rubbery elastic. Still, stress related contributions to the diffusion flux can be important and can cause inhomogeneous equilibrium in the gel under boundary constraints (Durning and Morman, 1993). Such contributions are neglected here as available data on diffusion coefficients in gelatin and related gels do not account for them either (Yapel et al., 1994; Price et al., 1977). Therefore, the diffusive mass flux j is taken to obey Fick's law with a concentration-dependent binary diffusion coefficient D

$$j \equiv \rho_p(v - v_p) = -\rho D \nabla w. \tag{8}$$

Stress in the solid-fluid mixture

Two general approaches have been used in developing CEs for mixtures of fluids and elastic solids. The first is based on mixture theory concepts. These theories are either phenomenological and utilize physically intuitive models for the forces on each component to relate transport and stress (Tanaka et al., 1973; Matsuo and Tanaka, 1988; Li and Tanaka, 1990; Thomas and Windle, 1982; Durning, 1985; Cox and Cohen, 1989; Doi and Onuki, 1992; Onuki, 1993; Wu and Peppas, 1993a,b), or based on rigorous rational thermodynamics frameworks (Crochet and Naghdi, 1966; Dunwoody, 1970; Kenyon, 1976a,b; Cohen and Metzner, 1986; Lustig, 1989) that guarantee consistency with the second law. In this approach the total stress is taken as the sum of partial stresses due to the polymer network and the penetrant fluid. Swelling is viewed as a strain caused by the stress that the penetrant exerts on the polymer network. Thomas and Windle (1982) and Durning (1985) identified the osmotic pressure as the swelling stress. This approach is useful mainly in swelling processes in which solvent activity is close to unity. It can predict syneresis effects and non-Fickian diffusion kinetics (Lustig, 1989). Its main disadvantage is that it requires CEs for partial quantities which may be unmeasurable.

The second approach is empirical (Larche and Cahn, 1982; Kim and Neogi, 1984): it requires a CE for the *total* mixture stress (accounting for both mechanical and swelling strains) rather than the individual partial stresses. The notion of a solid framework is still required, however, since elastic stresses are caused by the deformation of the polymer rather than that of the mixture. The resulting equations are isomorphic to those of thermoelasticity (Sih et al., 1986; Malvern, 1969) except when stress-induced diffusion is taken into account. This approach cannot predict equilibrium compositions, but requires them as input data; it has been applied mainly to drying processes. Durning and Morman's (1993) method straddles the boundary between phenomenological and mixture theory models. It does not invoke individual component balances, but is based on an entropy inequality with the diffusive flux being a constitutive quantity determined from the mixture's total free energy.

Here, we follow the mixture-theory approach of Kenyon (1976a,b) that provides a framework for CEs of mixtures of elastic solids and perfect fluids. According to Kenyon (1976b), in an *incompressible* mixture, the stress in the fluid is an isotropic pressure p_f, which induces a self-equilibrated pressure in the solid. On an area average basis, the pressure in the fluid is $\phi_w p_f$ and the self-equilibrated pressure in the solid is $\phi_p p_f$, where $\phi_w = \rho w/d_w$ and $\phi_p = \rho(1-w)/d_p$ are the volume fractions of solvent and polymer. The total stress in the mixture is then the sum of p_f, and the "contact stress" τ_p that arises from the macroscopic deformation of the solid (polymer network)

$$\boldsymbol{T} = -p_f \boldsymbol{I} + \tau_p \tag{9}$$

The contact stress is derived from the free energy density of the polymer network ψ_p: (cf. Kenyon, 1976b, Eq. 3.27)

$$\boldsymbol{\tau}_p = \rho_p \boldsymbol{c} \frac{\partial \psi_p}{\partial \boldsymbol{c}} \tag{10}$$

where $\boldsymbol{c} \equiv (\partial \boldsymbol{x}/\partial \boldsymbol{X})^T(\partial \boldsymbol{x}/\partial \boldsymbol{X})$ is the Finger tensor of the polymer network that relates the length of a small element in the deformed state $\boldsymbol{x}$ to its length in the undeformed state $\boldsymbol{X}$. Here we consider a simple model for the elastic free energy density of the form

$$\psi_p(I_1, I_2, I_3) = \phi_p \frac{\nu_e RT}{2}(I_1 - 3 - \ln I_3) \tag{11}$$

where

$$I_1 \equiv tr\boldsymbol{c}, \quad I_2 \equiv \frac{1}{2}\left(I_1^2 - tr\boldsymbol{c}^2\right), \quad I_3 \equiv \det \boldsymbol{c} = \left(\frac{\phi_p^0}{\phi_p}\right)^2 \tag{12}$$

are the basic invariants of tensor $\boldsymbol{c}$; ϕ_p^0 is the polymer volume fraction of the initial state, which is also assumed to be the relaxed state at which the crosslinks were introduced; ν_e is the number of crosslinks per unit volume of dry polymer, R is the gas constant, and T the absolute temperature. The resulting contact stress is

$$\boldsymbol{\tau}_p = \frac{\phi_p}{\phi_p^0} G_0 \boldsymbol{E} + \frac{\phi_p}{\phi_p^0}\left(\frac{K_0}{2} - \frac{G_0}{3}\right) \boldsymbol{I} tr\boldsymbol{E}, \quad \boldsymbol{E} \equiv \boldsymbol{c} - \boldsymbol{I} \tag{13}$$

where K_0 and G_0 are the bulk and shear modulus of the polymer network at the relaxed state, given by $G_0 = 2\nu_e RT = 3/2\, K_0$. Equation 16 is rubber elasticity (Treloar, 1975). Lustig's (1989) elastic model is similar but with $K_0 = B/C + 4\nu_e RT/3$, the first term on the righthand side arising from the (linear) compressibility of pure polymer chains. However, the contributions to the moduli from the macroscopic network elasticity and the microscopic chain compressibility are not additive (see Biot and Willis, 1957; Kenyon, 1976b, Eq. 3.22).

Nevertheless, in general, G_0 and K_0 need not be related as in the kinetic theory of rubber elasticity and should be measured independently.

The volumetric (second) term on the righthand side of Eq. 13 can be conveniently included in the isotropic pressure term of Eq. 9. Then the stress is given by

$$\boldsymbol{T} = -p'\boldsymbol{I} + \boldsymbol{\tau}, \qquad \boldsymbol{\tau} \equiv \frac{\phi_p}{\phi_p^0} G_0 \boldsymbol{E} \tag{14}$$

where $\boldsymbol{\tau}$ is the "extra" stress which also satisfies the incremental (differential) law

$$\hat{\boldsymbol{\tau}} \equiv \frac{\partial \boldsymbol{\tau}}{\partial t} + \boldsymbol{v}_p \cdot \nabla \boldsymbol{\tau} - \nabla \boldsymbol{v}_p \cdot \boldsymbol{\tau} - \boldsymbol{\tau} \cdot \nabla \boldsymbol{v}_p^T + \boldsymbol{\tau} \nabla \cdot \boldsymbol{v}_p = G \boldsymbol{D}_p,$$

$$G \equiv G_0 \frac{\phi_p}{\phi_p^0} \tag{15}$$

Here $\boldsymbol{D}_p \equiv (1/2)[\nabla \boldsymbol{v}_p + (\nabla \boldsymbol{v}_p)^T]$ is the deformation rate of the dry polymer network; the caret $\hat{}$ denotes the so-called Truesdell objective stress rate (hereafter referred to as the "UCT" rate), which is the upper convected maxwell (UCM) rate augmented with the term $\boldsymbol{\tau} \nabla \cdot \boldsymbol{v}_p$ that accounts for the changing polymer density (Eringen, 1962; for a molecular basis see also Edwards and Beris, 1990). More general incremental laws can be obtained if the shear and bulk moduli exhibit a power-law dependence on the polymer volume fraction (McEvoy et al., 1985). The proper differential law is then

$$\hat{\boldsymbol{\tau}} \equiv \frac{\partial \boldsymbol{\tau}}{\partial t} + \boldsymbol{v}_p \cdot \nabla \boldsymbol{\tau} + f(\boldsymbol{\tau}, \nabla \boldsymbol{v}_p) + \alpha \boldsymbol{\tau} \nabla \cdot \boldsymbol{v}_p = G \boldsymbol{D}_p,$$

$$G \equiv G_0 \left(\frac{\phi_p}{\phi_p^0} \right)^{\alpha}, \qquad f(\boldsymbol{\tau}, \nabla \boldsymbol{v}_p) \equiv -\nabla \boldsymbol{v}_p \cdot \boldsymbol{\tau} - \boldsymbol{\tau} \cdot \nabla \boldsymbol{v}_p^T \tag{16}$$

For $\alpha = 0$, Eq. 16 is equivalent to the UCM elastic law that does not take into account the change of moduli with polymer density. Such a material yields in network compression such as that accompanied by drying (see Results section). For general dependence of G on ϕ_p, Eq. 16 describes a class of nonlinear solid materials called "hypoelastic" which have a subtle difference from elastic materials: whereas the stress in an elastic material depends only on the current state of deformation, the stress in a hypoelastic material depends on the entire deformation path but not on the rate at which this path is traversed (Eringen, 1962). Although an elastic material with an invertible CE such as Eq. 15 is hypoelastic, a complicated relation must hold in order for a hypoelastic material to be elastic (see Noll, 1955; also Bernstein, 1960a,b; Simo and Pister, 1984).

In general, p' in Eq. 13 is not the mechanical pressure, $-tr(\boldsymbol{T})/3$, because $tr(\boldsymbol{\tau})$ is not zero. In order to be able to handle compressible mixtures in which the partial component densities depend on the stress, it is convenient to define a new pressure p so that $p = -tr(\boldsymbol{T})/3$ (Astarita and Marrucci, 1974, p. 35; Edwards and Beris, 1990)

$$\boldsymbol{T} = -\left(p + \frac{tr(\boldsymbol{\tau})}{3} \right) \boldsymbol{I} + \boldsymbol{\tau} \tag{17}$$

Compressible Gels. Although the mixture stress was developed here assuming incompressible components, the formulation has been already extended by Kenyon (1976b) to include pressure-dependent solid and fluid densities. In that case there is an extra isotropic term in the solid and total stresses

$$\frac{K_p}{f_s} \boldsymbol{I} \int f_s dp_f, \tag{18}$$

where K_p is the compressibility due to macroscopic volume change (at constant fluid pressure) and f_s is the pressure-dependent factor of the solid density. In the present formulation, however, the additional isotropic term (Eq. 18) can be included in the pressure term of Eq. 17, which makes the formulation valid for compressible components. Any effect of the additional term on the diffusion flux is neglected in this work but is addressed elsewhere (Powell et al., 1998a).

Empirical CE. Up to this point, stress CEs based only on mixture theory have been addressed. For comparison, the empirical approach gives the total stress in the mixture (such as by direct generalization of linear hygroelasticity)

$$\hat{T} = K_m \left[\nabla \cdot \boldsymbol{v}_p + \frac{1}{1-w} (\dot{w} + \boldsymbol{v}_p \cdot \nabla w) \right] \boldsymbol{I} + 2G_m \left(\boldsymbol{D}_p - \frac{\boldsymbol{I} \nabla \cdot \boldsymbol{v}_p}{3} \right) \tag{19}$$

Here, K_m and G_m are the bulk and shear modulus of the *entire mixture* rather than those of the polymer network alone. The first term in the righthand side of Eq. 19 accounts for the volumetric strain from a reference state that evolves continuously with solvent removal. For incompressible mixtures ($K_m \to \infty$), this term becomes indeterminate and again can be conveniently handled by a pressure. The total stress is then given by Eq. 9 but with $\boldsymbol{\tau}$ being now an "extra" stress satisfying

$$\hat{\boldsymbol{\tau}} = G \left(\boldsymbol{D}_p - \frac{\boldsymbol{I} \nabla \cdot \boldsymbol{v}_p}{3} \right) \tag{20}$$

Polymer velocity formulation

Because the CE (Eq. 16) involves only the polymer velocity $\boldsymbol{v}_p$, it is convenient to express all equations in terms of the same velocity by eliminating the mass average velocity $\boldsymbol{v}$ through the flux Eq. 8. The overall continuity equation, continuity of polymer, and solvent flux at the free surface become

$$\frac{\partial \rho}{\partial t} + \nabla \cdot (\rho \boldsymbol{v}_p) - \nabla \cdot \left(\frac{\rho D}{1-w} \nabla w \right) = 0 \tag{21}$$

$$\frac{\partial [\rho(1-w)]}{\partial t} + \nabla \cdot [\rho(1-w) \boldsymbol{v}_p] = 0 \tag{22}$$

$$\boldsymbol{n} \cdot \left(-\frac{D\rho}{1-w} \nabla w \right) = k_m H(w - w_\infty) \tag{23}$$

Next, the time derivative of ρ is expressed in terms of those of p and w, and the equations are written in an independ-

ently moving frame of reference (to be identified below as the finite-element mesh). That is, time derivatives $\partial/\partial t$ at a fixed location are transformed to time derivatives at fixed transformed coordinate in the new frame (denoted by an overdot) by using the identity

$$\frac{\partial \omega}{\partial t} = \dot{\omega} - \dot{x}\cdot\nabla\omega \tag{24}$$

With the relative velocity between the polymer and the new frame $c \equiv v_p - \dot{x}$, the stress CE, overall continuity, and continuity of polymer equations become ($\beta = 1$ invokes the empirical theory)

$$\dot{\tau} + c\cdot\nabla\tau + f(\tau, \nabla v_p) + \alpha\tau\nabla\cdot v_p = 2G\left(D_p - \frac{\beta}{3} I\nabla\cdot v_p\right) \tag{26}$$

$$\frac{\rho}{1-w}(\dot{w} + c\cdot\nabla w) - \nabla\cdot\left(\frac{D\rho}{1-w}\nabla w\right) = 0 \tag{27}$$

$$\nabla\cdot v_p + \frac{\partial \ln(\rho)}{\partial p}(\dot{p} + c\cdot\nabla p) + \left(\frac{\partial \ln(\rho)}{\partial w} - \frac{1}{1-w}\right)(\dot{w} + c\cdot\nabla w) = 0 \tag{28}$$

Finite Element Solution

Mesh generation

Essential to the finite-element solution of free boundary problems is the efficient and robust tessellation of the flow domain and unknown boundaries. Although a Lagrangian mesh that follows the motion of the polymer network would avoid the troublesome convective terms in the CE, it is unsuitable for the problems in this study because of the large deformation that the gel suffers in the course of drying. The method of choice here is the elliptic mesh generation system of Christodoulou and Scriven (1992), which produces meshes capable of following large deformations without significant deterioration of smoothness and orthogonality while allowing independent control of nodal point concentration (cf., Thompson et al., 1985). Details for choosing the necessary control parameters of this system can be found in the aforementioned (Christodoulou and Scriven, 1992) article.

Mixed formulations

Transient states of the system (Eqs. 3, 6, 26–28) combined with the two equations of the elliptic mesh generation system were computed by mixed finite-element methods that expand the various fields in terms of independent trial (basis) functions. Galerkin's method was used for the momentum, overall continuity and polymer continuity equations, whereas two upwinding methods were used for the CE. Velocity, pressure, extra stress, solvent concentration and nodal coordinates were expanded in two-dimensional trial functions: velocity and solvent concentration in nine-node biquadratic functions; pressure in three-node linear discontinuous functions for incompressible components; four-node bilinear continuous pressures are necessary for compressible mixtures as convective time derivatives of pressure appear explicitly in Eq. 28. Various functions were tested for the extra stress, as detailed below.

The nonlinear, differential-algebraic system of equations for the vanishing of the weighted residuals was obtained by multiplying each equation by the appropriate test function, integrating over the physical domain, and applying the divergence theorem to the momentum and diffusion equations. In axisymmetric problems the weighting functions were divided by the radial coordinate resulting in more uniform weighting of the residuals between regions close to and away from the axis. The weak forms of the overall continuity (combined with mass transfer at free surface), continuity of polymer, momentum, stress, and kinematic equations are

$$\int_A \frac{\rho}{1-w}(\dot{w} + c\cdot\nabla w)\phi dA - \int_A \frac{D\rho}{1-w}\nabla\phi\cdot\nabla w dA - \int_{\partial A} k_m(w_s - w_\infty)\phi d(\partial A) = 0 \tag{29}$$

$$\int_A \left[\nabla\cdot v_p + \frac{\partial \ln(\rho)}{\partial p}(\dot{p} + c\cdot\nabla p) + \left(\frac{\partial \ln(\rho)}{\partial w} - \frac{1}{1-w}\right)(\dot{w} + c\cdot\nabla w)\right]\pi dA = 0 \tag{30}$$

$$\int_A T\cdot\nabla\phi dA - \int_{\partial A} n\cdot T\phi d(\partial A) = 0 \tag{31}$$

$$\int_A \left[\dot{\tau} + c\nabla\cdot\tau + f(\tau, \nabla v_p) - 2G\left(D_p - \frac{\beta}{3} I\nabla\cdot v_p\right)\right]\bar{\psi} dA = 0 \tag{32}$$

$$\int_{\partial A} n\cdot c\phi ds = 0 \tag{33}$$

where π, ψ, and ϕ are the basis functions for pressure, extra stress, and velocity (ϕ is also used to expand solvent mass fraction and nodal coordinates) and G in Eq. 32 is given by Eq. 16. The hyperbolic nature of the stress equation was handled with either the consistent streamline upwind Petrov-Galerkin method (SUPG) or with the inconsistent Streamline Upwind method (SU), both of which add a small amount of stabilizing artificial diffusion along streamlines by making use of the modified weighting function (for details and the precise definition of k, see Marchal and Crochet, 1987)

$$\bar{\psi} = \psi + k v_p\cdot\nabla\psi \tag{34}$$

Essential boundary conditions were imposed by replacing the corresponding weighted residual equation with the desired variable specification.

Consistency of Mixed Formulations. As in the velocity-pressure (u-p) formulation of Newtonian flow, mixed finite-element formulations of viscoelastic flow are stable only for certain combinations of the trial functions. For instantaneously elastic CEs, Crochet (1982) showed that the momentum equation acts as a constraint on the CE, and for the Jacobian matrix of the system to be nonsingular, the extra stress should be derivable from the velocity field, setting a

lower limit on the number of extra stress unknowns per element. A more stringent requirement is satisfaction of the so-called LBB (or "inf-sup") consistency condition (Reddy, 1984), which, however, is difficult to apply for the complex problems addressed here. To satisfy this condition in the Newtonian limit, Marchal and Crochet (1987) showed that the set of extra stress functions should include that of the velocity gradient, a severe restriction requiring the extra stress functions to be discontinuous at interelement boundaries. Such discontinuity is incompatible with the convective terms in the CE.

The straightforward Mixed Finite Element (MFE1) method of Kawahara and Takeuchi (1977) uses continuous stress functions, but does not satisfy the LBB condition and does not reduce to the u-p formulation in the Newtonian limit. Three other formulations, the MFE2 of Crochet and Keunings (1982), the MFE3 of Mendelson et al. (1982) and the more successful Elastic-Viscous-Split-Stress (EVSS) method of Rajagopalan et al. (1990) explicitly introduce the velocity into the momentum equation and do reduce to the u-p formulation in the Newtonian limit. However, none of these is applicable to the hypoelastic limit. Marchal and Crochet's (1987) 4×4 stress subelements (see also Crochet and Legat, 1992) satisfy the LBB condition in the Newtonian limit (Fortin and Pierre, 1989), but are computationally expensive. Even more expensive is the "product approximation," with the stress-velocity products as independent unknowns and discontinuous stress, first implemented for hypoelastic materials by Liu (1986, 1988) and Liu et al. (1991).

Guenette and Fortin (1995) extended the benefits of the EVSS method to CEs that are based on a conformation tensor, which also makes it applicable to hypoelastic materials. Following Arnold and Brezzi (1993), they expanded the deformation rate in terms of continuous functions and augmented the momentum equation with a regularizing term proportional to the difference between the deformation rate $\boldsymbol{D}_p$ and its smoothed counterpart $\boldsymbol{d}$

$$\nabla\cdot\left[\boldsymbol{\tau}-p\boldsymbol{I}+2\gamma\left(\boldsymbol{D}_p-\boldsymbol{d}\right)\right]=\boldsymbol{0} \tag{35}$$

$$\boldsymbol{d}=\boldsymbol{D}_p \tag{36}$$

The velocity is thus explicitly introduced in the momentum equation and any restrictions on the stress basis functions are bypassed. Clearly, Eq. 36 and the additional term in Eq. 35 are meaningful only at the discrete level. The weak form of Eq. 36 is

$$\int_A\left(\boldsymbol{d}-\boldsymbol{D}_p\right)\nabla\psi dA=0 \tag{37}$$

Bilinear continuous functions can now be used for both the extra stress and $\boldsymbol{d}$, making this method very efficient, especially for multimode viscoelastic CEs. More recently, Liu et al. (1997) introduced the Discrete Elastic-Viscous-Split-Stress-Gradient formulation (DEVSS-G), a variant of the Guenette-Fortin (GF) method that smooths all components of the velocity gradient tensor $\nabla\boldsymbol{v}_p$, and uses them in the stress CE. This method satisfies the compatibility requirement that the stress space include the space of the velocity gradient.

Effect of Solvent Viscosity. Instantaneously elastic models like Eq. 15 are often plagued by artificial changes of type or "Hadamard instability" causing unbounded growth of short wave disturbances and loss of the well-posedness (or evolutionary character) of the initial-boundary value problem with disastrous computational consequences. Equation-type analysis of the coupled set (Van der Zanden and Hulsen, 1988) established that in order to maintain "evolutionarity," a certain tensor χ that reduces to the tensor $\boldsymbol{\tau}+\mu_p/\lambda\boldsymbol{I}$ $(=\boldsymbol{\tau}+G\boldsymbol{I})$ for the UCM model should be positive definite. Evolutionarity is guaranteed for the UCM, lower convected Maxwell (LCM), and UCT models (Joseph, 1990) in the continuum limit but not in their numerical approximations (Dupret et al., 1985).

Addition of solvent viscosity to instantaneously elastic Maxwell-type models turns them into retarded elasticity models and regularizes the coupled set formed by the momentum, continuity equations and CEs (Joseph, 1990; Van der Zanden and Hulsen, 1988). The new set does not exhibit a change of type even when the material properties depend on the deformation rate. More importantly, numerical loss of positive definiteness of χ does not necessarily result in Hadamard instability and ill-posedness. Accordingly, in our calculations, a minute amount of Newtonian solvent stress τ_s was added to the total stress T in Eq. 14, where

$$\boldsymbol{\tau}_s=\mu_s\boldsymbol{D}_p, \tag{38}$$

Here, μ_s is a small numerical parameter.

Time integration

Area integrals in the weighted residuals (Eqs. 29–33, 37) were evaluated by nine-point Gaussian quadrature and line integrals by three-point quadrature. As in the Newtonian case, the result of integration is a system of differential and algebraic equations of index two (Petzold, 1982a), $\boldsymbol{R}(t,y,\dot{y})=0$, for the vector of time-dependent coefficients $\boldsymbol{y}=[u_i,\ v_i,\ p_j,\ w_i,\ \tau_{xxm},\ \tau_{xym},\ \tau_{yym},\ d_{xx},\ d_{xy},\ d_{yy},\ x_l,\ y_l]^T$ for 2-D Cartesian geometries, or for $\boldsymbol{y}=[u_i,\ v_i,\ p_j,\ w_i,\ \tau_{rrm},\ \tau_{rzm},\ \tau_{zzm},\ \tau_{\theta\theta m},\ d_{rr},\ d_{rz},\ d_{zz},\ d_{\theta\theta},\ x_l,\ y_l]^T$ for axisymmetric geometries. The time-stepping method of choice was the differential-algebraic system solver DASSL (Petzold, 1982b), based on a variable time-step, variable order backward difference method. DASSL uses Newton's method for finding the discretized equations and requires a linear combination of the Jacobian and mass matrices which was approximated using the finite difference formula

$$\left(\frac{\partial\boldsymbol{R}}{\partial\boldsymbol{y}}+\omega\frac{\partial\boldsymbol{R}}{\partial\dot{\boldsymbol{y}}}\right)_{ij}\cong\frac{R_i\left(\boldsymbol{y}+\epsilon\boldsymbol{e}_j,\dot{\boldsymbol{y}}+\epsilon\omega\boldsymbol{e}_j\right)-R_i\left(\boldsymbol{y},\dot{\boldsymbol{y}}\right)}{\epsilon} \tag{39}$$

where $\boldsymbol{e}_j$ is the unit vector in the jth direction and ϵ is a small number taken as a sum of a relative term proportional to $\|\boldsymbol{y}\|$ and an absolute term independent of $\|\boldsymbol{y}\|$. Hood's (1976) frontal solver was used for finding the solution of the resulting linear equations.

Initial Conditions. While differential CEs allow imposition of arbitrary initial stress, this stress must be compatible with the initial displacement for a unique solution to exist (Eringen, 1962). Here, it is assumed that no frozen-in stresses remain after gelation and that gravity effects are negligible;

accordingly, initial conditions were taken at zero stress. In general, as is suitable for index-II differential-algebraic systems, consistent initial conditions and time derivatives close to an arbitrary initial state can be calculated by taking two first-order backward difference steps with suppressed time truncation error control (see Christodoulou and Scriven, 1992). Some additional modifications that are known to enhance the performance of DASSL in Newtonian flow problems (Petzold and Loetstedt, 1986) were also incorporated.

Applications

We have applied the model to study drying of polymer gels coated on rigid substrates in three geometries, all of considerable practical importance: uniformly coated films, around rigid cylindrical particles in free-standing films, and around spherical particles in coated films. We tried CEs based on Eq. 26 with the UCM ($\alpha = 0$) and UCT ($\alpha = 1$) rates, and in combination with the mixture theory or with the empirical laws. The component densities are taken constant, that is, compressibility and volume change on mixing were ignored making weight fractions numerically equal to volume fractions. Equations 26–28 and 35–36 were made dimensionless by measuring length in units of initial thickness L_0, stress and pressure in units of shear modulus G_0, time in units of L_0^2/D_0, and velocity in units of D_0/L_0. The resulting dimensionless parameter is the *Biot* number $Bi \equiv k_m HL_0/D_0$, which is the ratio of the mass-transfer resistances in the air and in the gel, and in the presence of solvent viscosity (retardation), a second dimensionless number, $\beta_s = \mu_s D/GL_0^2$. The gel is assumed to be stress-free in the initial state with $w = w_0$, and is then exposed to air which would be in equilibrium with a gel of $w = w_\infty$.

Drying of a uniformly coated gel layer

The first application is drying of a uniform gel layer coated on a flat, rigid substrate as depicted in Figure 1. This test case serves to validate the visco/hypoelastic stress model, and to investigate the predicted stress growth with various objective stress rates. The mass-transfer resistance in the gas phase is assumed to be much larger than that in the gel thus eliminating any gradients in the gel. A macroscopic solvent mass balance across the thickness of the coating combined with the boundary condition (Eq. 23) gives

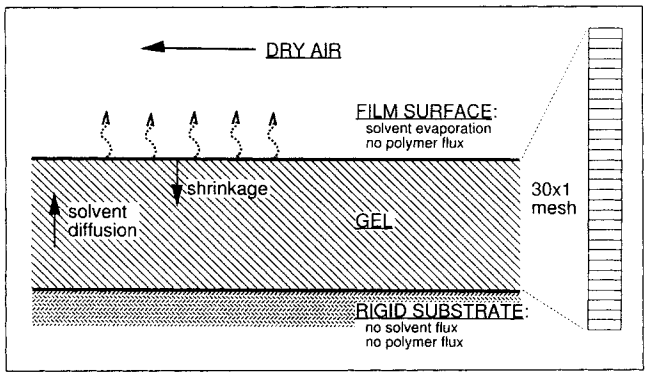

Figure 1. Idealized system and initial finite-element mesh for drying of a uniformly coated layer.

$$\frac{d(\rho wV)}{dt} = \rho k_m A(w - w_\infty) \tag{40}$$

here $V = AL = AL_0(1 - w_0)/(1 - w)$ is the volume of the coating, A is its surface area; L and w are the current thickness and (uniform) solvent mass fraction of the coating; L_0 and w_0 are the corresponding initial values. Equation 40 is integrated analytically to yield an algebraic equation for $w = w(t)$ (in dimensionless form)

$$\left[\frac{w - w_\infty}{w_0 - w_\infty}\frac{1 - w_0}{1 - w}\right] - \frac{1}{1 - w_\infty}\left(\frac{1 - w_0}{1 - w} - 1\right) = Bit \tag{41}$$

The deformation of the polymer network vanishes in all but the thickness direction, and the strain is $E_{yy} = [(1 - w_0)/(1 - w)]^2 - 1$. For $\beta = 0$, the contact stress is then given from Eq. 16.

$$\tau_{yy} = G_E(1 - w)^\alpha\left[\left(\frac{1 - w_0}{1 - w}\right)^2 - 1\right] \tag{42}$$

The same problem was solved with the 2-D finite element model with periodic boundary conditions that make it effectively 1-D. A 30×1 element mesh was used with Galerkin's method (no upwinding), linear discontinuous pressure, and continuous biquadratic extra stress. Figure 2 shows that the evolution of $w(t)$ and $\tau_{yy}(t)$ from Eqs. 41 and 42 agrees well with that computed with the finite-element model. Independent validation of the diffusion equations was also performed, but this is straightforward and details are not reported here.

From the computed τ_{yy}, it is easy to calculate the total in-plane stress T_{xx}. In the absence of capillary effects, the total stress normal to the free surface is equal to the ambient pressure, which is taken to be atmospheric (pressure datum), so $T_{yy} = -p + \tau_{yy} = 0$, and therefore $p = \tau_{yy}$ everywhere in the film. Moreover, because $\tau_{xx} = \tau_{zz} = 0$, by *definition* $T_{xx} = T_{zz} = -p = -\tau_{yy}$. The predicted growth of T_{xx} over time for various values of the constitutive parameters is shown in Fig-

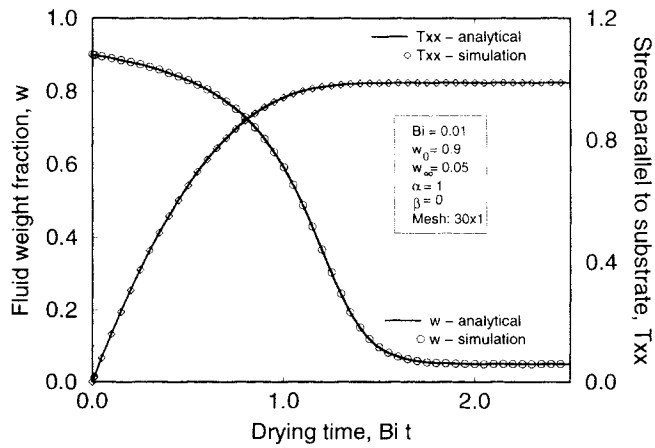

Figure 2. Analytical and numerical predictions of stress and concentration histories for drying of a uniformly coated layer.

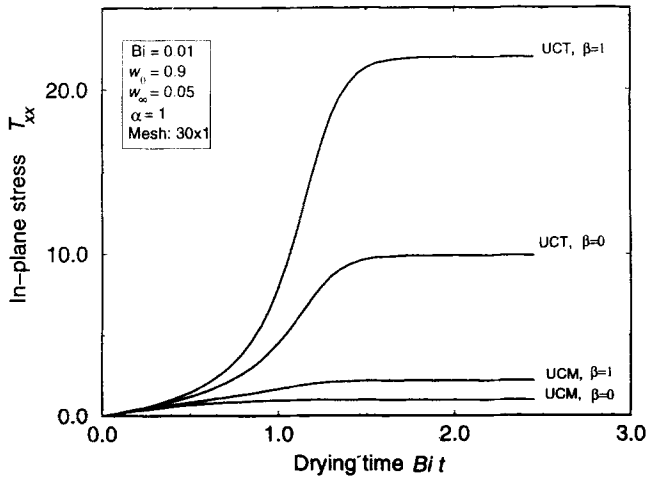

Figure 3. Predicted time evolution of the in-plane stress T_{xx} with various constitutive laws.

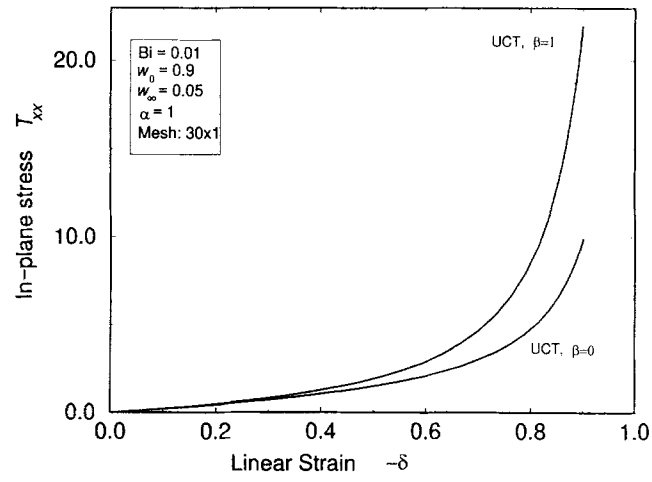

Figure 5. In-plane stress T_{xx} as a function of linear strain $\delta = (L - L_0)/L_0$ predicted by the UCT-type constitutive laws.

ure 3 and, as a function of the linear measure of deformation $\delta = (L - L_0)/L_0$, in Figures 4 and 5.

With the UCM law, $T_{xx} = -\tau_{yy}$ grows linearly at first but soon saturates at one, long before the film is completely dry. The reason is that these stresses are generated by a compressive polymer velocity field. Indeed, a hypoelastic UCM solid yields under compression and cannot support a compressive stress higher than its shear modulus (Eringen, 1962). Therefore, such a model is suitable only for small deformations.

With the empirical UCM law ($\alpha = 0$, $\beta = 1$), T_{xx} keeps increasing beyond unity with no sign of yield. Part of T_{xx} is now contributed by the nonvanishing in-plane "contact" stress τ_{xx}, which is tensile and therefore does not exhibit hypoelastic yield (Eringen, 1962). With the UCT mixture law ($\alpha = 1$, $\beta = 0$), T_{xx} grows faster as the modulus now increases with polymer mass fraction. The stress growth is linear with γ initially, but accelerates at large deformations. With the empirical law ($\beta = 1$), the growth of T_{xx} deviates from linearity earlier, resulting in even higher residual stress. Clearly, the

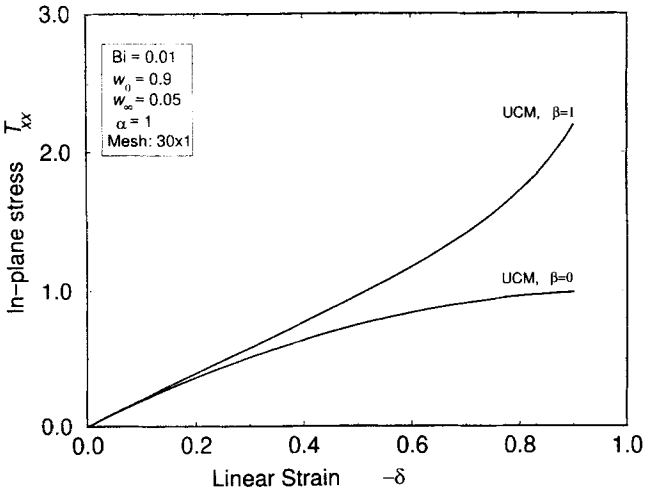

Figure 4. In-plane stress T_{xx} as a function of linear strain $\delta = (L - L_0)/L_0$ predicted by the UCM-type constitutive laws.

parameters α and β have to be chosen for the material at hand from independent rheological measurements. Unless otherwise noted, in the rest of the examples below we used $\alpha = 1$ and $\beta = 0$ (equivalent to rubber elasticity).

Cylindrical particle in a clamped layer

A more interesting problem is that of a rigid particle included in a polymeric film suspended at the edges but not attached to a substrate (such as during stretching or drying in a tenter-frame oven). Depending on the composition of the film, the polymer might be a simple melt (such as poly-ethylene-terephthalate), a solvent laden gel (such as poly-vinyl-fluoride), or a reactive solvent laden gel (such as poly-imide). The particles are added to provide surface roughness that eases film transport, or to reduce the gloss of the film, or they may be chemically functional (such as flame retardants). Here, we consider the area around a single particle included in a gel cast film being dried. Because two axes of symmetry exist, the computational domain reduces to only a quarter of the entire particle shown in Figure 6 along with the imposed boundary conditions.

This more complicated geometry allows assessing various numerical methods for treating the CE. With the standard MFE1 and continuous biquadratic stress, Newton iteration failed at $t = 1.13$ (dimensionless time units), when the film was still wet ($w = 0.037$ at the free surface above the particle and $w = 0.13$ at the substrate). Upwinding (SUPG, SU), product approximation or rate of momentum formulations and mesh refinement resulted in no improvement. In every case, around $t = 1.15$, a very sudden instability occurred as stresses grew large: severe spatial oscillations ("wiggles") first appeared in the velocity field and were shortly followed by loss of convergence of the Newton iteration.

The determinant of the *dimensionless* tensor $\chi \equiv \tau + I$ was monitored during the integration. It was found that it turned negative at $t = 0.95$ (see Figure 7) and was shortly followed by the appearance of wiggles in the velocity field failure of the Newton iteration. The integration was then repeated with a minute amount of solvent viscosity $\beta_s = 0.03$. This sup-

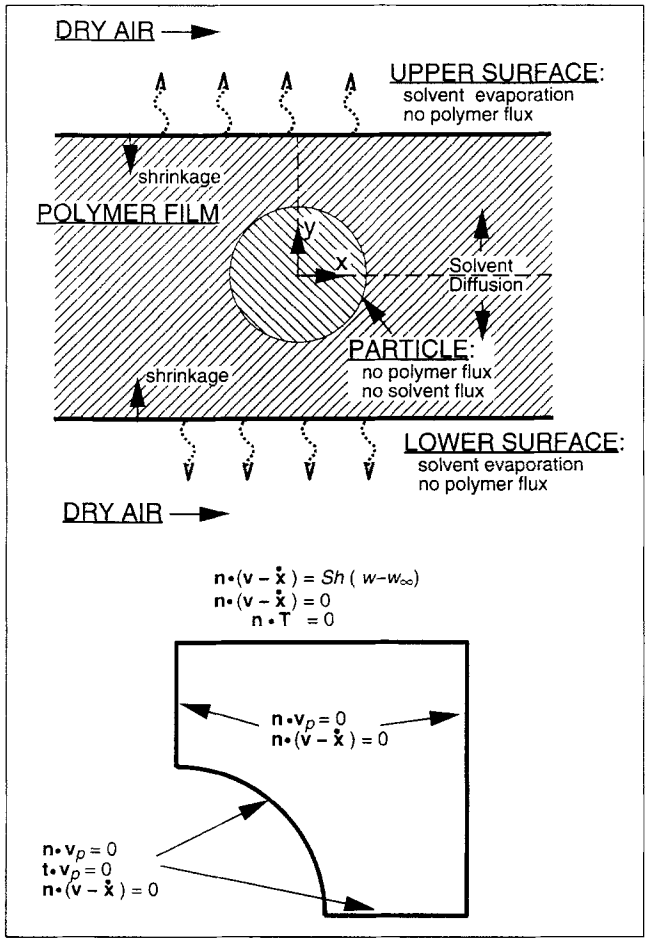

Figure 6. Idealized system and computational domain with boundary conditions for model of drying around a cylindrical particle in a free-standing polymer film.

pressed the instability with the UCM law and the computation proceeded until the film dried completely. The UCT law, however, still failed at $t = 1.3$, when w at the top of the coating was 0.058 and at the bottom 0.082.

The best results were obtained with the GF and DEVSS-G formulations with $\gamma = 1$ and $\beta_s = 0.03$; no spurious oscillations were evident and the gel dried completely with either the UCM or UCT rates. DEVSS-G resulted in a somewhat smoother stress field, but time integration was about 10% slower than with GF. Using $\beta_s = 0$ also resulted in smooth fields but the time integration became extremely (about 50 times) slower. Figure 8 shows the computed free surface and finite element mesh evolution during drying of a UCT material.

Figure 9 shows, on three successively refined meshes (of 14×6, 20×8, and 30×12 elements) and at $t = 0.75$, predictions of the pressure p and of the Von Mises stress function $T_{vm} \equiv \sqrt{(\tau - Itr(\tau)/3):(\tau - Itr(\tau)/3)}$, which measures the likelihood of mechanical failure. The reason for choosing this intermediate time to report the computed fields is that the extreme strains in the gel at later times cause the stress to lose some of its smoothness. The maximum and minimum values of these variables converge with mesh refinement.

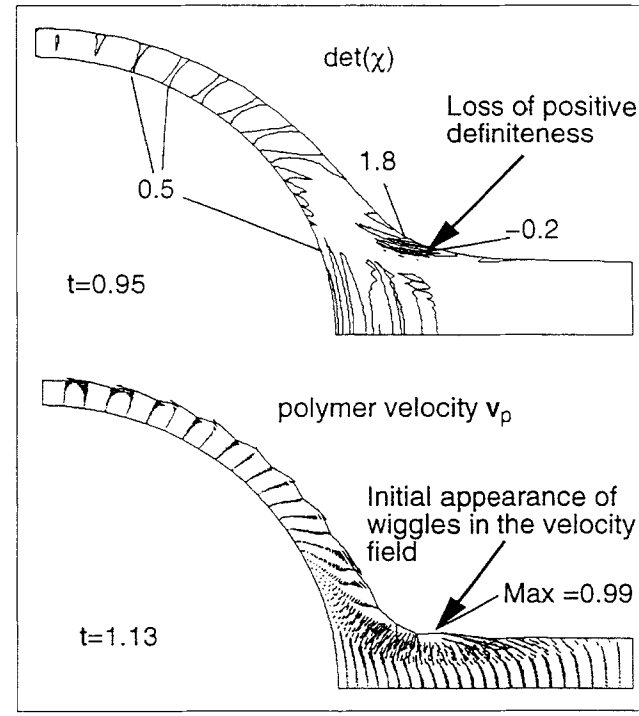

Figure 7. Loss of positive definiteness of det(χ) followed by appearance of wiggles in the velocity field and breakdown of the computation with the MFE1 formulation.

Contours of the total stress components and of T_{vm} in the final dry state are shown in Figure 10. The in-plane component T_{xx} is tensile (positive) along the horizontal plane of symmetry and rises away from the particle. The out-of-plane

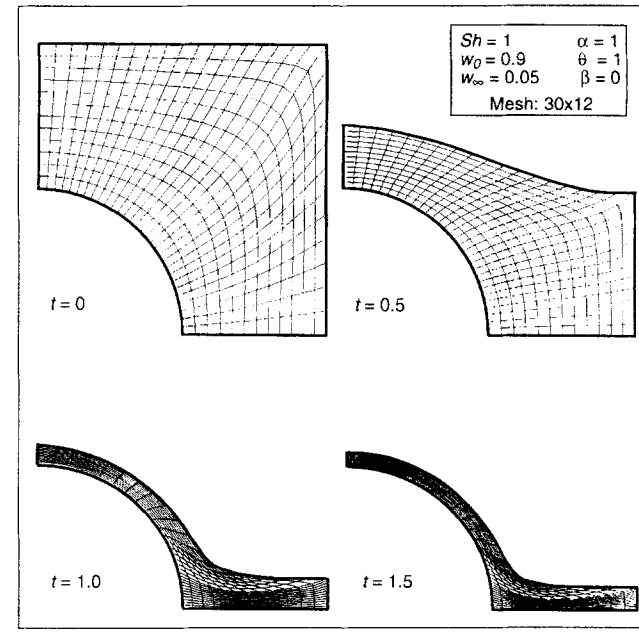

Figure 8. Free surface and finite-element mesh evolution during drying around a cylindrical particle in a free-standing (symmetric) polymer film predicted using the DEVSS-G formulation.

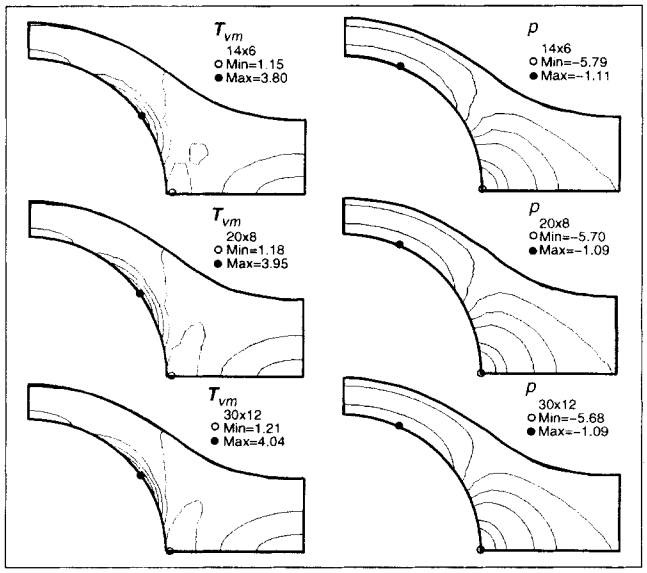

Figure 9. Convergence study of the numerical solution for pressure and Von Mises stress function for drying around a cylindrical particle in a free-standing film at $t = 1$.

component T_{yy} is also tensile over most of the region, but reaches its maximum on the particle surface. The shear component T_{xy} also reaches its largest magnitude on the particle surface at a latitude of 45°. The net effect is a maximum in T_{vm} on the surface of the particle around a latitude of 30°. This is where mechanical failure is most likely.

Spherical particle in two-layer photographic film ("starry night" defect)

The ultimate goal of this work was to study a defect that occurs in the manufacture of black and white photographic films used in graphic arts. Typical graphic arts photographic films are multilayer structures in which one (or more) silver halide bearing photographic layer is protected by an overcoat

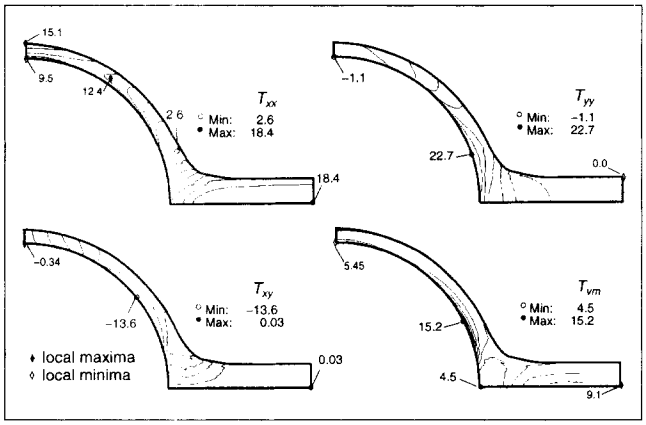

Figure 10. Predicted stress tensor components and Von Mises stress function at the end of drying (5% solvent) around a cylindrical particle in a free-standing film.

layer. In the wet state the layers are typically 50–100 μm thick after coating. They are immediately chilled into reversible gels that can withstand the impinging air in the dryer without visible surface deformation, and then dried to a thickness of the order of 5 μm. In order to achieve surface roughness and other desired properties in subsequent film processing, inert solid particles are usually added to the overcoat layer. The size of these particles is typically 0.1–10 μm in diameter. Thus, although the particles enter the dryer smaller than the wet coating thickness they produce a significant distortion in the dry film. During drying, these particles may penetrate the photographic underlayer causing microscopic holes in the developed image. The appearance of affected film, viewed under a microscope, gives rise to the common name "starry night." Starry night can be controlled by lowering the line speed (that is, the drying rate) or it can be compensated by increasing the silver halide content of the film. Because of the high cost of silver, the line speed is frequently limited by the starry night constraint. Predictably, published discussions of the starry night defect have been limited to the patent literature (Anonymous, 1982; Heigold and Hoskyns, 1979; Whitmore and Coryell, 1968; Bagchi et al., 1989) and professional society conferences (Lightfoot and Christodoulou, 1990; Christodoulou and Lightfoot, 1992).

Because of the low temperature of chilling, no significant amount of drying occurs before the coated sol has gelled; thus, any complications of the sol-gel transition can be decoupled from the drying problem. Here the polymer gel was modeled as a nonlinear elastic or hypoelastic solid. The mean distance between matte particles in the coatings is of the order of 10 to 15 particle radii, large enough so that particle-particle interaction can be safely neglected. An idealized system considered here is a cylindrical piece of two-layer photographic coating with a single spherical particle in the top layer. Because of the axisymmetry, only half of the particle was simulated. The computational region along with imposed boundary conditions is also shown in Figure 11.

With the DEVSS-G formulation and $\beta_s = 0.03$, integration proceeded smoothly until the film dried completely. Figure 12 shows that the elliptically-generated meshes successfully track the motion of the physical region without excessive element distortion. Figures 13 and 14 show contour plots of the predicted stress components and of the residual Von Mises stress function T_{vm}. Both the in-plane stress T_{rr} and the peeling component T_{zz} are tensile over much of the region, attaining maxima on the surface of the particle. Both turn compressive, although smaller, beneath the particle and along its lower surface. The shear stress T_{rz} also attains maxima on the particle. The hoop stress $T_{\theta\theta}$ has a tensile maximum at the north pole, and a compressive maximum at the south. The net effect is a maximum in T_{vm} on the surface of the particle just above the equator.

The computed residual stresses not only show where the material may fail, but also help to uncover the mechanism of starry night: because of the adhesion constraint, a tensile stress parallel to the particle surface develops in the gel which in combination with the curvature of the particle gives rise to a capillarity-like downward force that pushes the particle into the lower photographic layer (see Figure 15).

With a working model that can predict particle penetration into the photographic layer, it is now possible to investigate

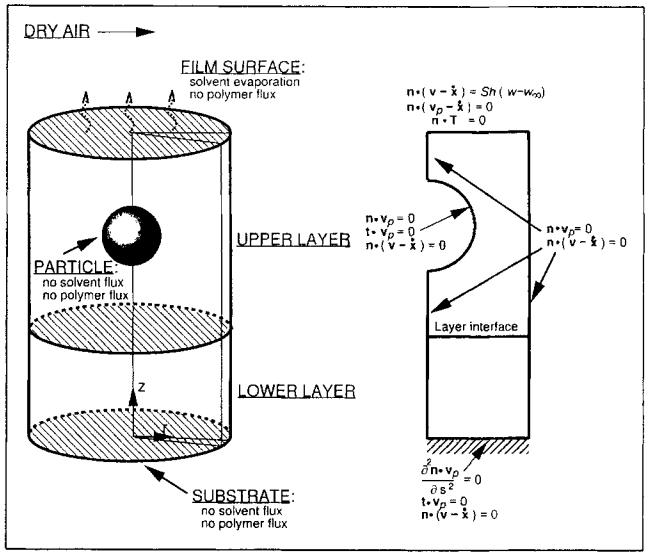

Figure 11. Idealized system and computational domain with imposed boundary conditions for model of drying around a spherical particle in a polymer layer coated onto a substrate ("starry night" defect problem).

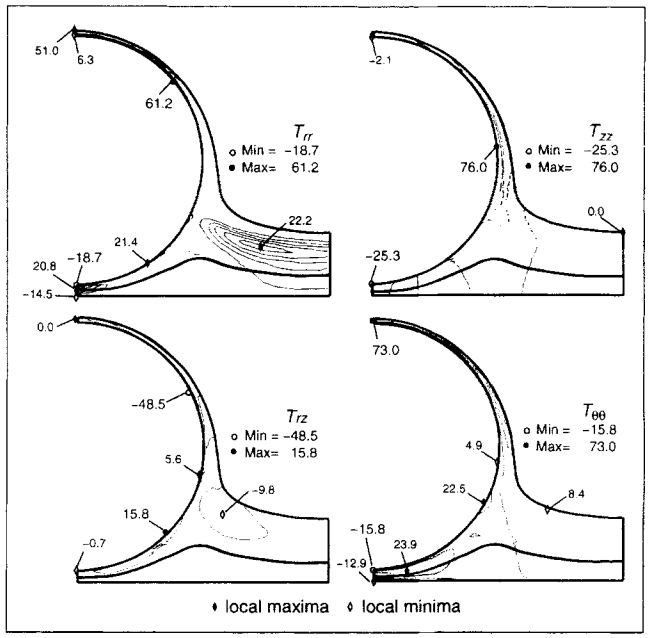

Figure 13. Predicted stress tensor components at equilibrium (end of drying) for the starry night problem.

the effect of varying the rheological properties of the two layers. Figure 16 shows that the final penetration of the particle into the lower (photosensitive) layer increases by a factor of three as the modulus ratio of the lower to the upper layer is reduced tenfold from 1 to 0.1. The UCM model has been used to describe the elasticity of the gel in this case. For the same case, Figure 17 shows the effect of modulus ratio on the time evolution of the minimum lower layer thickness (that is, the lower layer thickness at the south pole of the particle). Figure 18 shows, again for the lower layer, the effect of modulus ratio on the ratio of minimum thickness to normal thickness (away from the particle) and on the ratio of maximum thickness (at the ridge of the crater formed by the lower layer) to the minimum thickness. The last two thickness ratios are expected to better quantify the starry night defect. Clearly, reducing the lower layer modulus reduces the minimum lower layer thickness and therefore exacerbates the defect. These results are in accord with the mechanism of the defect uncovered above with the help of the model.

In reality, the gel along the upper half of the particle is expected to dry and stiffen more rapidly than the gel in the

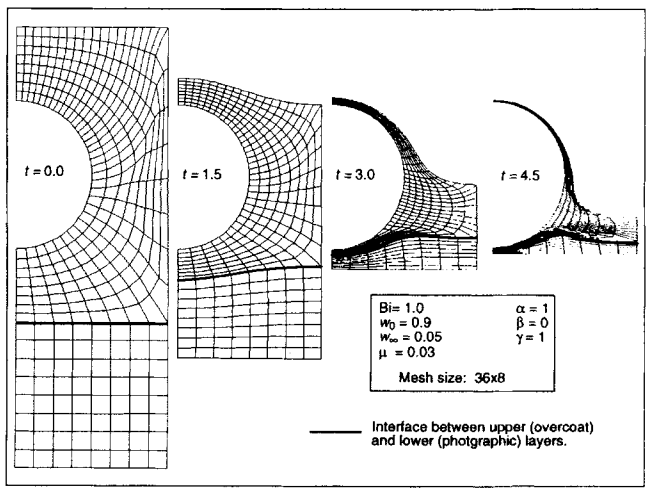

Figure 12. Predicted free surface and finite-element mesh evolution during drying for the starry night problem.

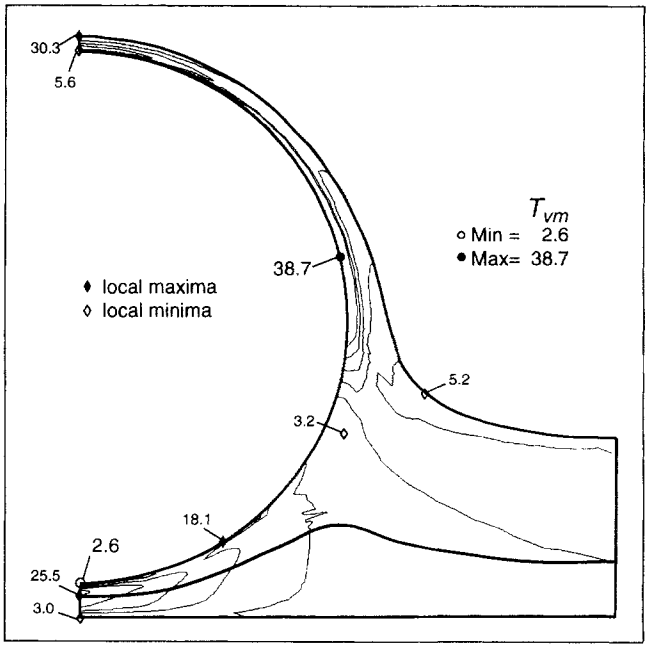

Figure 14. Predicted Von Mises stress function at equilibrium (end of drying) for the starry night problem.

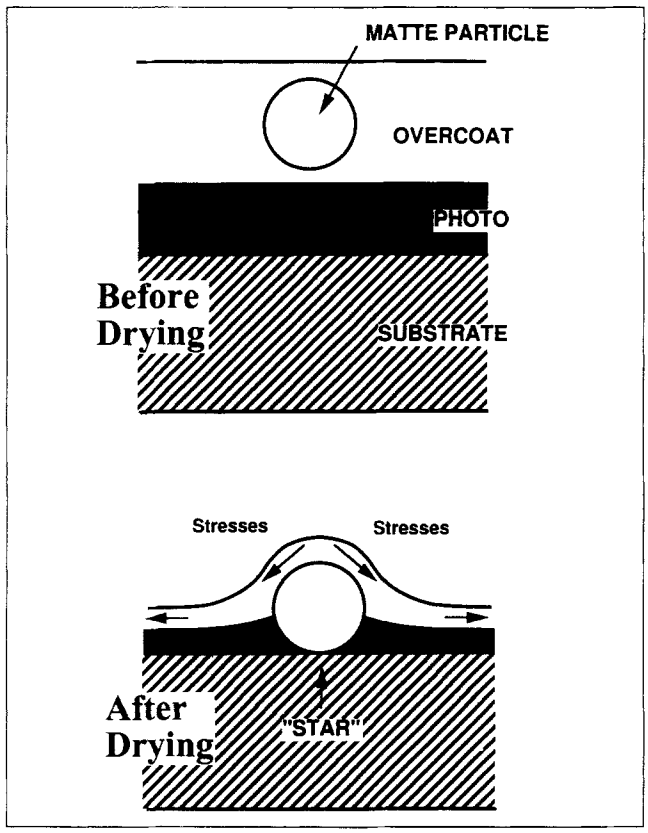

Figure 15. Mechanism of the starry night defect.

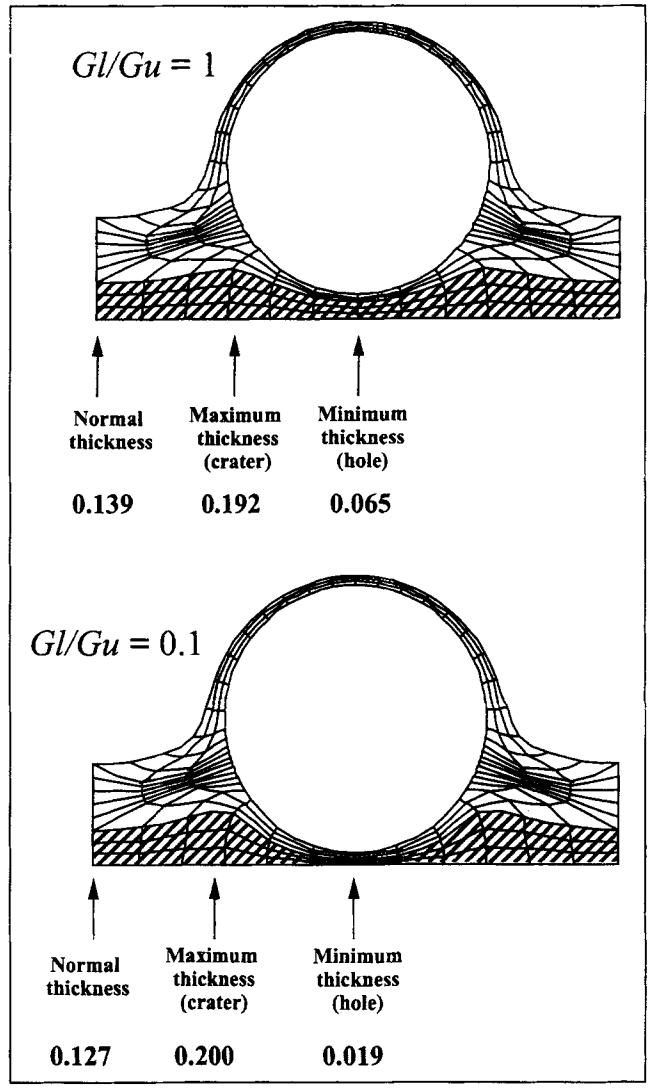

Figure 16. Final particle penetration into the lower layer computed with the UCM model for two lower-to-upper layer modulus ratios.

lower half. It is possible that the wetter gel in the lower half yields, causing additional particle penetration into the lower layer. This can be further exacerbated when simultaneous hardening reactions take place that usually further stiffen the drier regions of the gel (see Croome, 1976).

Conclusions and Future Directions

A model is proposed for predicting stress growth and defect formation in drying of polymer films encountered in photographic and automotive applications. The model describes solvent loss accompanied by large deformation of the polymer network. The latter is treated as a nonlinear solid described by a differential CE of the hypoelastic type. Mass transfer and thermodynamic nonlinearities were not included in order to simplify the search for a robust numerical method. The governing equations were put in terms of the polymer network velocity and discretized on an elliptically generated finite-element mesh. Among various mixed-interpolation methods tested, the technique of Guenette and Fortin (1995) and its modification by Liu et al. (1997) were found the most stable and efficient.

The model was applied to predict residual solvent, deformation, stress development, and defect formation in drying of uniform films coated on relatively rigid substrates, free standing films (as in tenter-frames), and films with particuclusions. Stress predictions have aided in uncovering the mechanism of "starry night," a common drying defect in the photographic industry.

The model proposed here can be improved in several ways. The constant diffusion, distribution, and mass-transfer coefficients that were used in the examples can be readily substituted with more realistic parameters based on the Flory-Huggins theory as reported elsewhere (Powell et al., 1998b). Including the volumetric part of the network stress in the pressure (that is, using Eq. 14 rather than Eq. 10) eliminates the need for the osmotic bulk modulus K. The resulting theory, however, cannot predict equilibrium solvent concentration, which must now be measured independently. With the omission of stress-induced diffusion mentioned above, these predicted equilibrium states are homogeneous. Nevertheless, such an approach is useful in solving drying problems in which residual solvent fraction is minute but the gel does not go through its glass transition, or when the osmotic elastic modulus of the gel is much greater than its shear elastic modulus (cf. Durning and Morman, 1993). By contrast, to predict polymer swelling, the *network* stress should be balanced with the solvent osmotic pressure to determine

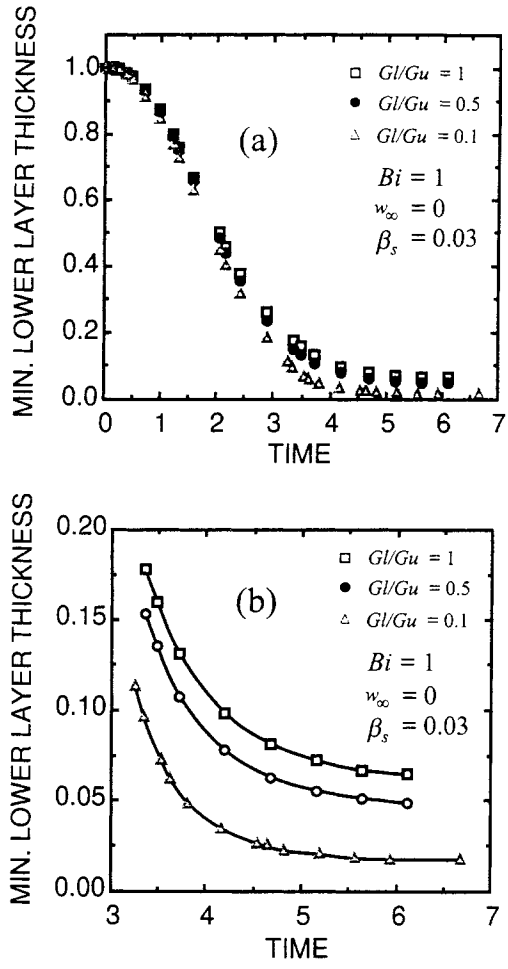

Figure 17. Effect of modulus ratio on the time evolution of the minimum lower-layer thickness: (a) global view and (b) expanded view near the end of drying.

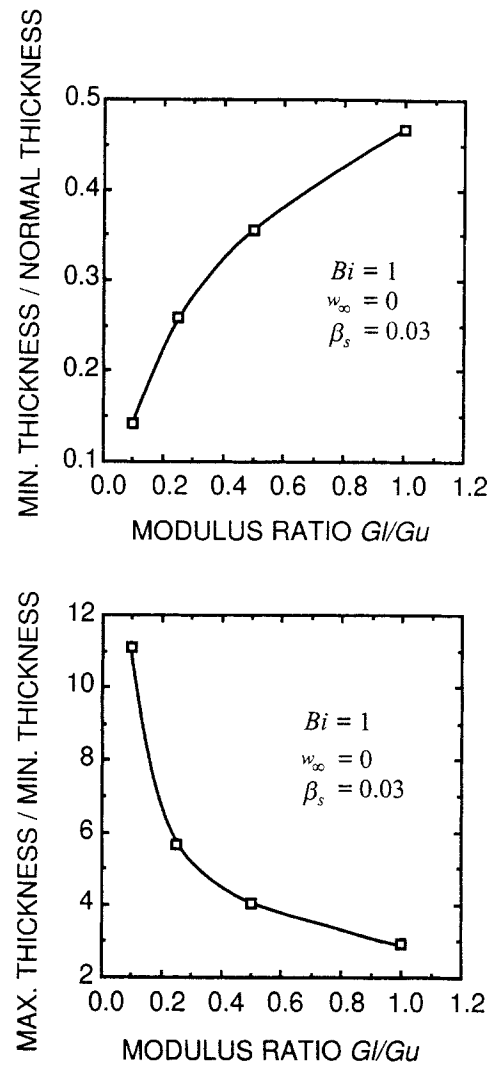

Figure 18. Effect of modulus ratio on final lower-layer ratios of (a) minimum thickness to normal thickness, and (b) maximum thickness to minimum thickness.

the equilibrium solvent fraction. It is then necessary to keep the CE in terms of the contact stress τ_p and the osmotic modulus K (see Powell et al., 1998b).

The issue of the thermodynamic consistency of the CE and the diffusion flux is avoided by excluding stress-induced contributions to the diffusion flux (Eq. 8), thus decoupling stress and diffusion. As long as a CE with positive dissipation is used (Leonov, 1987, 1992; Kwon and Leonov, 1995), the total dissipation will be positive.

With the Finger tensor appearing explicitly in Eq. 14, more general hyperelastic laws (such as Mooney-Rivlin materials) can readily be implemented. Stress- and pressure-induced diffusion can be incorporated in the diffusive flux (Eq. 8), but those would raise the issue of thermodynamic consistency in the resulting fully coupled problem. These issues are taken up in upcoming publications (Powell et al., 1998a,b). Viscoelasticity (stress relaxation) can also be included, such as by solving

$$\frac{\tau}{\lambda(\phi_p)} + \overset{\circ}{\tau} = G(\phi_p)E \qquad (43)$$

in lieu of Eq. 16. Here $\lambda(\phi_p)$ is the relaxation time of the polymer network. In the vicinity of the glass transition, the relaxation time changes by orders of magnitude and leads to sharp concentration fronts propagating at constant speed, skinning, and anomalous diffusion kinetics. These are addressed in forthcoming publications along with extensions to multicomponent solvents and simultaneous chemical hardening reactions by building on the work of Lustig et al. (1992).

Literature Cited

Anonymous, "Use of Monodisperse Matte to Improve Resistance of Photographic Film to Handling and Coating Defects," *Res. Discl.*, **216**, 109 (1982).

Arnold, D. N., and F. Brezzi, "Some New Elements for the Reissner-Mindlin Plate Model," *Boundary Value Problems for Partial Differential Equations and Applications*, J. L. Lions and C. Baiocchi, eds., Masson, New York, p. 287 (1993).

Astarita, G., and G. Marrucci, *Principles of Non-Newtonian Fluid Mechanics*, McGraw-Hill, New York (1974).

Bagchi, P., M. D. Sterman, and H. M. Low, "Photographic Element Having Polymer Particles Covalently Bonded to Gelatin," U.S. Patent 4,855,219 (1989).
Bernstein, B., "Hypo-Elasticity and Elasticity," *Arch. Rational Mech. and Analysis*, **6**, 90 (1960a).
Bernstein, B., "Relations between Hypo-Elasticity and Elasticity," *Trans. Soc. Rheol.*, **4**, 23 (1960b).
Bierwagon, G. P., "Film Formation and Mudcracking in Latex Coatings," *J. Coatings Tech.*, **51**, 117 (1979).
Biot, M. A., and D. G. Willis, "The Elastic Coefficients of the Theory of Consolidation," *J. Appl. Mech.*, **24**, 594 (1957).
Brinker, C. J., and G. W. Scherer, *Sol-Gel Science: The Physics and Chemistry of Sol-Gel Processing*, Harcourt, Brace and Jovanovich, Boston (1990).
Ceaglske, N. H., and O. A. Hougen, "Drying Granular Solids," *Ind. Eng. Chem.*, **29**, 805 (1937).
Christodoulou, K. N., and L. E. Scriven, "Discretization of Free Surface Flows and Other Free Boundary Problems," *J. Comp. Phys.*, **99**, 39 (1992).
Christodoulou, K. N., and E. J. Lightfoot, "Stress-Induced Defects in the Drying of Thin Films," Paper 46c, AIChE Meeting, New Orleans (Mar. 29–Apr. 2, 1992).
Cohen, E. D., "Coatings: Going Beneath the Surface," *Chem. Eng. Prog.*, **86**, 19 (1990).
Cohen, E. D., E. B. Gutoff, and E. J. Lightfoot, "A Primer on Forming Coatings," *Chem. Eng. Prog.*, **86**, 30 (1990).
Cohen, Y., and A. B. Metzner, "Diffusion of Macromolecules: A Constitutive Theory," *Chem. Engr. Commun.*, **41**, 73 (1986).
Cox, R. W., and D. S. Cohen, "A Mathematical Model for Stress Driven Diffusion in Polymers," *J. Polym. Sci., Polym. Phys. Ed.*, **27**, 589 (1989).
Crochet, M. J., and P. M. Naghdi, "On Constitutive Equations for Flow of Fluid through an Elastic Solid," *Int. J. Engng. Sci.*, **4**, 383 (1966).
Crochet, M. J., "The Flow of a Maxwell Fluid around a Sphere," in *Finite Elements in Fluids*, R. H. Gallagher, D. H. Norrie, J. T. Oden, and O. C. Zienkiewicz, eds., Wiley, New York, **4**, 573 (1982).
Crochet, M. J., and R. Keunings, "On Numerical Die-Swell Calculation," *JNNFM*, **10**, 85 (1982).
Crochet, M. J., and V. Legat, "The Consistent Streamline-Upwind/Petrov-Galerkin Method for Viscoelastic Flow Revisited," *JNNFM*, **42**, 283 (1992).
Croll, S. G., "The Origin of Residual Stress in Solvent Cast Thermoplastic Coatings," *J. Appl. Polym. Sci.*, **23**, 847 (1979).
Croome, R. J., "The Kinetics of the Development of Rigidity in Gelatin Gels," *Photographic Gelatin II*, R. J. Cox, ed., Academic Press, New York (1976).
Doi, M., and A. Onuki, "Dynamic Coupling Between Stress and Composition in Polymer Solutions and Blends," *J. Phys. II. France*, **2**, 1631 (1992).
Dunwoody, N. T., "A Thermomechanical Theory of Diffusion in Solid-Fluid Mixtures," *Arch. Rat. Mech. Anal.*, **38**, 348 (1970).
Durning, C. J., "Differential Sorption in Viscoelastic Fluids," *J. Poly. Sci., Polym. Phys. Ed.*, **23**, 1831 (1985).
Durning, C. J., and K. N. Morman, Jr., "Nonlinear Swelling of Polymer Gels," *J. Chem. Phys.*, **98**, 4275 (1993).
Dupret, F., J. M. Marchal, and M. J. Crochet, "On the Consequence of Discretization Errors in the Numerical Calculation of Viscoelastic Flow," *JNNFM*, **18**, 173 (1985).
Edwards, B. J., and A. N. Beris, "Remarks Concerning Compressible Viscoelastic Fluid Models," *JNNFM*, **36**, 411 (1990).
Eringen, A. C., *Nonlinear Theory of Continuous Media*, McGraw-Hill, New York (1962).
Fortin, M., and R. Pierre, "On the Convergence of the Mixed Method of Crochet and Marchal for Viscoelastic Flows," *Comput. Meth. Appl. Mech. Engng.*, **73**, 341 (1989).
Guenette, R., and M. Fortin, "A New Mixed Finite Element Method for Computing Viscoelastic Flows," *JNNFM*, **60**, 27 (1995).
Heigold, F. R., and W. F. Hoskyns, "Photographic Element Containing a Light Absorbing Matting Agent," U.S. Patent 4,172,731 (1979).
Hood, P., "Frontal Solution Program for Unsymmetric Matrices," *Int. J. Num. Meth. Engng.*, **10**, 379 (1976).
Joseph, D. D., *Fluid Dynamics of Viscoelastic Liquids*, Springer-Verlag, New York (1990).
Kawahara, M., and N. Takeuchi, "Mixed Finite Element Methods for Analysis of Viscoelastic Fluid Flow," *Comput. Fluids*, **5**, 33 (1977).
Kenyon, D. E., "Thermostatics of Solid-Fluid Mixtures," *Arch. Rat. Mech. Anal.*, **62**, 117 (1976a).
Kenyon, D. E., "The Theory of an Incompressible Solid-Fluid Mixture," *Arch. Rat. Mech. Anal.*, **62**, 131 (1976b).
Kim, M., and P. Neogi, "Concentration-Induced Stress Effects in Diffusion of Vapors through Polymer Membranes," *J. Appl. Poly. Sci.*, **29**, 731 (1984).
Keunings, R., "Simulation of Viscoelastic Fluid Flow," in *Computer Modeling for Polymer Processing*, C. L. Tucker III, ed., Hanser, New York (1989).
Kwon, Y., and A. I. Leonov, "Analysis of Simple Constitutive Equations for Viscoelastic Liquids," *JNNFM*, **58**, 25 (1995).
Larche, F., and J. W. Cahn, "A Linear Theory of Thermochemical Equilibrium of Solids Under Stress," *Acta. Metall.*, **21**, 1051 (1973).
Larche, F. C., and J. W. Cahn, "The Effect of Self-Stress on Diffusion in Solids," *Acta Matall.*, **30**, 1835 (1982).
Leonov, A. I., "On a Class of Constitutive Equations for Viscoelastic Liquids," *JNNFM*, **25**, 1 (1987).
Leonov, A. I., "Analysis of Simple Constitutive Equations for Viscoelastic Liquids," *JNNFM*, **42**, 323 (1992).
Li, Y., and T. Tanaka, "Kinetics of Swelling and Shrinkage of Gels," *J. Chem. Phys.*, **92**, 1365 (1990).
Lightfoot, E. J., and K. N. Christodoulou, "Starry Night and Drying," Paper 81h, AIChE Meeting, Orlando, FL (Mar. 18, 1990).
Liu, A. W., D. E. Bornside, R. C. Armstrong, and R. A. Brown, "Viscoelastic Flow of Polymer Solutions around a Periodic, Linear Array of Cylinders: Comparisons of Predictions for Microstructure and Flow Fields," *JNNFM*, in press (1997).
Liu, W. K., T. Belytschko, and H. Chang, "An Arbitrary Lagrangian-Eulerian Finite Element Method for Path-Dependent Materials," *Comput. Meth. Appl. Mech. Eng.*, **58**, 227 (1986).
Liu, W. K., H. Chang, J. S. Chen, and T. Belytschko, "Arbitrary Lagrangian-Eulerian Petrov-Galerkin Finite Elements for Non-Linear Continua," *Comput. Meth. Appl. Mech. Eng.*, **68**, 259 (1988).
Liu, W. K., H. Chang, J. S. Chen, T. Belytschko, and Y. F. Zhang, "Adaptive ALE Finite Elements with Particular Reference to External Work Rate on Frictional Interface," *Comput. Meth. Appl. Mech. Eng.*, **93**, 189 (1991).
Lustig, S. R., "A Continuum Thermodynamics Theory for Transport in Polymer Fluid Systems," PhD Thesis, Purdue Univ., West Lafayette, IN (1989).
Lustig, S. R., J. M. Caruthers, and N. A. Peppas, "Continuum Thermodynamics and Transport Theory for Polymer Fluid Mixtures," *Chem. Eng. Sci.*, **47**, 3037 (1992).
Malvern, L. E., *Introduction to the Mechanics of a Continuous Medium*, Prentice Hall, Englewood Cliffs, NJ (1969).
Marchal, J. M., and M. J. Crochet, "A New Mixed Finite Element for Calculating Viscoelastic Flow," *JNNFM*, **26**, 77 (1987).
Matsuo, E. S., and T. Tanaka, "Kinetics of Discontinuous Volume-Phase Transition of Gels," *J. Chem. Phys.*, **89**, 1695 (1988).
McEvoy, H., S. B. Ross-Murphy, and A. H. Clark, "Large Deformation and Ultimate Properties of Biopolymer Gels: 1. Single Biopolymer Component Systems," *Polymer*, **26**, 1483 (1985).
Mendelson, M. A., P. W. Yeh, R. A. Brown, and R. C. Armstrong, "Approximation Error in Finite Element Calculation of Viscoelastic Fluid Flows," *JNNFM*, **10**, 31 (1982).
Noll, W., "On the Continuity of Solid and Fluid States," *J. Rat. Mech. Anal.*, **4**, 3 (1955).
Nowacki, W., *Thermoelasticity*, 2nd ed., Pergamon Press, Oxford (1986).
Onuki, O., "Theory of Phase Transition in Polymer Gels," *Adv. in Poly. Sci.*, T. Tanaka, ed., **109**, 63, Springer-Verlag, New York (1993).
Perera, D. Y., "Internal Stress in Latex Coatings," *J. Coatings Tech.*, **56**, 111 (1984).
Petzold, L. R., "Differential/Algebraic Equations are not ODE's," *SIAM J. Sci. Stat. Comput.*, **3**, 367 (1982a).
Petzold, L. R., "A Description of DASSL: A Differential/Algebraic System Solver," *AND82-8637*, Sandia National Laboratories, Livermore, CA (1982b).
Petzold, L. R., and P. Loetstedt, "Numerical Solution of Nonlinear

Differential Equations with Algebraic Constraints II: Practical Implications," *SIAM J. Sci. Stat. Comput.*, **7**, 720 (1986).
Powell, R. W., K. N. Christodoulou, and I. G. Kevrekidis, "Non-Simple, Multicomponent Mixture Theory for Diffusion of Fluids in Polymers," *Chem. Eng. Sci.*, in press (1998a).
Powell, R. W., K. N. Christodoulou, and I. G. Kevrekidis, "Solvent Transport and 2-D Stress Development in Polymers: A Computer-Assisted Study," *Chem. Eng. Sci.*, in press (1998b).
Price, E. P., S. Wang, and I. H. Romdhane, "Extracting Effective Diffusion Parameters from Drying Experiments," *AIChE J.*, **43**, 1925 (1997).
Rajagopalan, D., R. C. Armstrong, and R. A. Brown, "Finite Element Methods of Steady, Viscoelastic Flow Using Constitutive Equations with a Newtonian Viscosity," *JNNFM*, **36**, 159 (1990).
Reddy, J. N., *Applied Functional Analysis and Variational Methods in Engineering*, McGraw-Hill, New York (1984).
Sato, K., "The Internal Stress of Coating Films," *Prog. Org. Coat.*, **8**, 143 (1980).
Scherer, G. W., "Theory of Drying," *J. Amer. Ceram. Soc.*, **73**, 3 (1990).
Sih, G. C., J. G. Michopoulos, and S. C. Chou, *Hygrothermoelasticity*, Martinus Nijhoff Publishers, Dordrecht (1986).
Simo, J. C., and K. S. Pister, "Remarks on Rate Constitutive Equations for Finite Deformation Problems: Computational Implications," *Comput. Meth. Appl. Mech. Eng.*, **46**, 201 (1984).
Tanaka, T., L. O. Hocker, and G. B. Benedek, "Spectrum of Light Scattered from a Viscoelastic Gel," *J. Chem. Phys.*, **59**, 5151 (1973).
Thomas, N. L., and A. H. Windle, "A Theory of Case-II Diffusion," *Polymer*, **23**, 529 (1982).
Thompson, J. F., Z. U. A. Warsi, and W. C. Mastin, *Numerical Grid Generation*, Elsevier, New York (1985).
Treloar, L. R. G., *The Physics of Rubber Elasticity*, Oxford Univ. Press, London (1975).
Van der Zanden, J., and M. Hulsen, "Mathematical and Physical Requirements for Successful Computations with Viscoelastic Fluid Models," *JNNFM*, **29**, 93 (1988).
Vrentas, J. S., C. M. Jarzebski, and J. L. Duda, "A Deborah Number for Diffusion in Polymer-Solvent Systems," *AIChE J.*, **21**, 894 (1975).
Vrentas, J. S., J. L. Duda, and W. J. Huang, "Regions of Fickian Diffusion in Polymer-Solvent Systems," *Macromol.*, **19**(6), 1718 (1986).
Whitmore, K. R., and G. M. Coryell, "Photographic Compositions Containing Combination of Soft and Hard Matting Agents," U.S. Patent 3,411,607 (1968).
Wu, J. C., and N. A. Peppas, "Modeling of Penetrant Diffusion in Glassy Polymers with an Integral Sorption Deborah Number," *J. Polym. Sci., Part B: Polymer Physics*, **31**, 1503 (1993a).
Wu, J. C., and N. A. Peppas, "Numerical Simulation of Anomalous Penetrant Diffusion in Polymers," *J. Appl. Poly. Sci.*, **49**, 1845 (1993b).
Yapel, R. A., J. L. Duda, X. Lin, and E. D. von Meerwall, "Mutual and Self-Diffusion of Water in Gelatin: Experimental Measurement and Predictive Test of Free-Volume Theory," *Polymer*, **35**, 2411 (1994).

Manuscript received Apr. 8, 1997, and revision received Apr. 1, 1998.